ISSN (Print) 1226-1750
ISSN (Online) 2233-6656
Journal of Magnetics 25(2), 215-222 (2020) https://doi.org/10.4283/JMAG.2020.25.2.215

Enhancement of the Packing Fraction of Iron-Based Soft Magnetic Amorphous Powders by Bimodal Powder Mixing

Jungjoon Kim[1], Yeonjoo Lee[1,2], Dohun Kwon[2], Hwijun Kim[2], and Hyunjoo Choi[1]*

[1]*School of Materials Science and Engineering, Kookmin University, Seoul 02707, Republic of Korea*
[2]*Division of New Materials Engineering, Korea Institute of Industrial Technology (KITECH), Incheon 21999, Republic of Korea*

(Received 30 January 2020, Received in final form 13 May 2020, Accepted 15 May 2020)

In this study, iron-based amorphous powders with two different sizes, which are the average sizes of 18.92 μm and 74.69 μm, were mixed to increase the powder packing fraction and resulting soft magnetic properties. By varying the mixing ratio, the powder packing fraction was experimentally measured and also estimated by the Desmond model and the computational simulation on the basis of the discrete element method (DEM). As a result, the DEM simulation exhibited higher validity compared to the Desmond model possibly because it accounts for the interaction between the powders, such as repulsion and aggregation, which are not considered in the Desmond equation. Finally, the maximum powder packing fraction of 73.86 % was achieved when the powders were mixed at the ratio of 5:3 (~25 μm: 45~63 μm). This ratio produced an increase of 32.5 % for coercivity and 17.8 % for saturated magnetization compared to the case of 100 % large powders with a 74.69 μm average diameter.

Keywords : soft magnetic, amorphous powder, packing fraction, simulation, discrete element method

1. Introduction

Soft magnetic materials were essential for the development of the early industrial applications of electricity; currently, these materials are a very important industrial product with an approximately 1.1 % market growth rate [1]. These materials are used in many devices such as communication equipment, electric-generating facilities, power-converting parts, electromagnetic wave shielding materials, and magnetic sensors [2-7]. The miniaturization of these devices required the development of high-performance soft magnetic materials with good reliability. Recently, amorphous materials have attracted considerable attention because a decrease in the crystal size results in a decrease in the coercivity, which means that minimum coercivity can be obtained in amorphous state [8]. Furthermore, the good magnetic properties of Fe-based amorphous materials (e.g., low coercivity, high permeability, and low core loss) can be maintained even at high frequencies owing to the disordered atomic arrangement of amorphous materials [9-12]. Specifically, amorphous materials in a powder form are of interest owing to their capacity to produce parts with complex morphologies with three-dimensional uniform magnetic properties [13, 14].

In powder-based magnetic materials, the packing fraction (i.e., the volume occupied by number of particles in a given volume) considerably affects magnetic properties. The coercivity and magnetization can change in proportion to the packing fraction of the products, and an increase in the fraction of the nonmagnetic region (e.g., void, grain boundary, pores, and phase boundary) may result in the deterioration of magnetic properties [15]. Therefore, the packing of spherical particles has been extensively studied for both soft and hard magnetic materials [16-19]. Powder with binomial distribution has been reported to be beneficial to powder packing compared to powder with monodisperse distribution [20], which simultaneously improves magnetic properties. In addition, when the electromagnetic wave shielding material in a powder form is mixed with the polymer binder, the electromagnetic wave shielding ability can be improved by improving the filling rate of the powder [21]. Therefore, research on improving the powder packing density of soft magnetic properties is important for various industrial fields ranging from energy-converting parts to electromagnetic

*Corresponding author: Tel: +82-2-910-4287
Fax: +82-2-910-4320, e-mail: hyunjoo@kookmin.ac.kr

shielding markets.

Research on the packing behavior of fine nonmetallic powders or hard magnetic powder has been actively conducted [22-30]. Furthermore, many studies used simulations based on random sequential addition (RSA), computational fluid dynamics (CFD), and discrete element method (DEM) to accurately grasp the filling behavior and increase the filling rate [31-34]. Recently, it has been reported that the packing fraction can be increased by about 16-23 % compared to a single powder by filling with mixed powder through the DEM-based computational simulation approach [32]. However, validation of computational approaches for predicting the packing behaviors of soft magnetic powders using experimental tests are still insufficient.

In this study, the change in powder packing behavior depending on various average particle size and particle size distribution was experimentally measured for Fe-based amorphous powders. In addition, the experimental results were compared with those of the Desmond model [35] and showed the effect of particle size distribution on the filling rate and computer modeling on the basis of the discrete element method (DEM) by accounting for the influence of physical interactions between powders.

2. Experimental

2.1. Sample preparation

The Fe–Cr–Si–B–C amorphous powder was produced by water atomization at Korea Institute of Industrial Technology (KITECH). A mixture of pure Fe, Cr, Si, B, and C (≥ 99.5 % purity) ingots was melted in a magnesia crucible in a high-frequency induction furnace at 1400 ℃. The density of the cast master alloy was approximately 6.28 g/cm^3. The cast master alloy was extruded into a bar shape to easily insert and re-melt it in the water-atomization equipment. The melt was atomized to produce an amorphous powder by passing through a 3 mm nozzle in the jet of Ar gas under an 80 bar pressure. The water was also sprayed at a 180 bar pressure at the outlet of the melt to achieve rapid cooling and produce amorphous powder. Then, the powder was dried in an oven for 12 h. The composition of the manufactured powder is shown in Table 1. The dried powder was passed through 25, 45, and 63 μm sieves to separate the powder by particle size. Powders with the diameter of 25 μm or smaller and powders with the diameter of 45-63 μm were used as initial powders and named S- and L-powders, respectively. Here, the maximum powder size was set to 63 μm to avoid partial crystallization of the powder during the given atomizing process. To observe the change in packing fraction by mixing powders of different sizes, a powder mixture was prepared using the weight ratios of 8:0-0:8. It has been reported that the closest packing can be achieved at a mixing ration of 1:7 [32], and in the present study, the optimal packing ratio was tried to be found by changing this ratio from 0:8 to 8:0.

Table 1. Nominal composition of L- and S-powders.

Soft magnetic powder	Fe	Cr	Si	B	C
at %	72.2	2.2	10.8	10.8	4

2.2. Characterization

A laser particle size analyzer (LPSA, Mastersizer 2000E, Malvern Instrument, UK) was used to analyze the particle size distribution of the powder, and field emission scanning electron microscopy (FE-SEM, JSM 7410F, JEOL Co., Japan) was used to analyze the shape of the powders.

The lattice structure of the Fe-based amorphous powders was characterized by X-ray diffraction (XRD) with a CN2301 (Rigaku, Japan) using CuKα (λ = 1.5405 Å). The samples were scanned over an angular range of 30-60° with a step size of 0.05° and a scan speed of 0.02°/min. During the XRD analysis, the sample was rotated to observe the general lattice. The diffractometer was set at 40 kV working voltage and 200 mA working current with a 2 mm slit size.

To measure the angle of repose, a funnel with an orifice with a diameter of 2.5 mm and a con angle of 30° was used. The center of the funnel and the horizontal plate were matched and positioned so that the distance between the tip of the funnel and the plate was 25 mm. Then, each initial powder and mixed powder was flown through the funnel to allow the powder to accumulate on the plate. After the experiment, the powder formed a triangular shape, and the image was acquired with a camera and analyzed by the image J software.

2.3. Calculation of the packing fraction

Each initial powder and mixed powder were analyzed, and the theoretical calculations and computational simulation were performed by analyzing the results.

First, we calculated the packing fraction using the Desmond model to perform the theoretical calculations. Recently, Desmond has presented a model that can simply predict the packing fraction of powder as a function of polydispersity and skewness.

$$\phi_{RCP} = \phi^*_{RCP} + c_1\delta + c_2 S\delta^2 \quad (1)$$

Where ϕ_{RCP} is the packing fraction of the powder to be obtained, and ϕ^*_{RCP} is the packing fraction when the

powder has a single distribution. ϕ^*_{RCP}, c_1, and c_2 are the experimentally measured constants. In this study, ϕ^*_{RCP}, c_1, and c_2 were 0.57, 0.0658, and 0.0857, respectively. Then, polydispersity and skewness, which considerably affect packing fraction, can be defined by the following equation.

$$\delta = \sqrt{(\Delta R^2)} / < R > \quad (2)$$

$$S = < \Delta R^3 > < \Delta R^2 >^{3/2} \quad (3)$$

Polydispersity is a value that is obtained by dividing the standard deviation of the powder radius by the radius of the average powder; polydispersity is a factor that indicates the degree of the distribution of deviations on the basis of the average value. The larger the polydispersity of the particle size distribution, the larger is the variation of the powder and thus the wider is the particle size distribution. Skewness is the sum of the cubes of deviations divided by the cube of the standard deviation; skewness is a factor that indicates the direction in which the distribution is skewed or the degree of asymmetry. It has a value of 0 when the left and right parts are symmetrical; skewness has a positive value when the tail of the distribution is stretched to the right compared to the symmetrical distribution; skewness has a negative value when the tail of the distribution is stretched to the left compared to the symmetrical distribution. In addition, an increase in the absolute value of the skewness increases the asymmetry of the distribution.

To simulate the packing behavior of the powder, EDEM (DEM Solution, UK), which is the DEM program, was used. DEM is a numerical method developed by Cundall and Strack that analyzes the interaction of particles with an external system at each time step; DEM allows to determine and trace particle movement [36]. When spherical particles contact each other, the contact forces can be derived from the material deformation, which depends on the specific material properties. We used the Edinburgh elasto-plastic adhesion model provided by the EDEM software to calculate the packing fraction. The model uses stochastic calculations and predicts the behavior of contacts between particles using various variables such as constant pull-off force, contact plasticity ratio, and particle properties. Therefore, the properties of the measured powder were applied to the computational simulation. In addition, after collecting the data by measuring the angle of repose of the actual powders, the characteristics of the powder in simulation were fitted with a focus on the behavior and flow of the powder-to-powder contact.

3. Results and Discussion

Figure 1 shows the morphology of the obtained powder after being classified according to the size of the powders by sieves sized 25, 45, and 63 μm. Each powder had a diameter of 25 μm or smaller and 45-63 μm. Most particles had spherical shapes to reduce the surface area because the liquid-state alloy was exposed to strong water pressure and was also rapidly cooled during the water-atomizing process. In addition, when the powder was manufactured via the water-atomization process, many satellite powders were present in the powder, which adversely affected the flow or packing; however, there were small quantities of both powders on the surface; thus, these powders did not have a considerable effect. For the S-powder, the use of the sieve with a 25-μm pore size showed that the powder contained very small particles that could not be classified using the sieve with the pore size of 25 μm or smaller. However, for powder classified as 45-63 μm, the size of the particles exhibited a uniform distribution. Particles with long shapes were sometimes observed. These particles could pass in a direction perpendicular to the sieve during the distribution process.

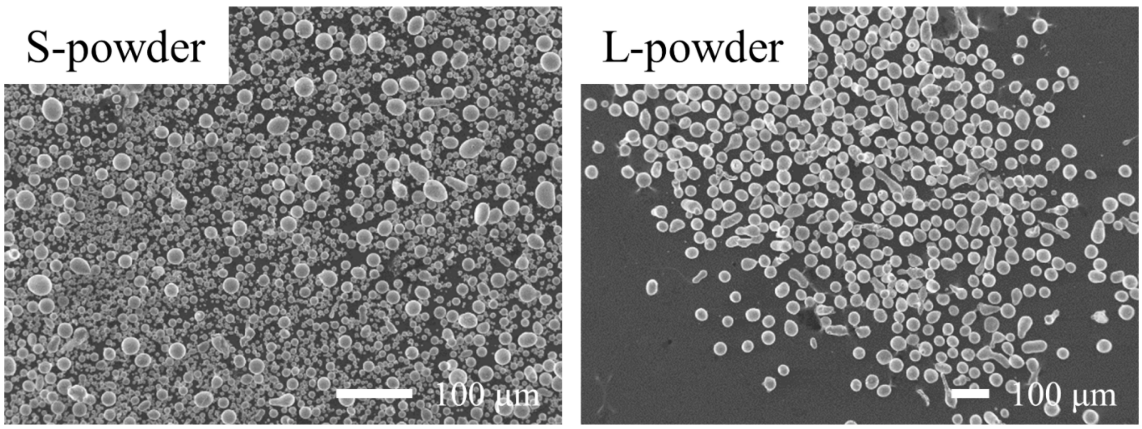

Fig. 1. Morphologies according to the size classification of the powder.

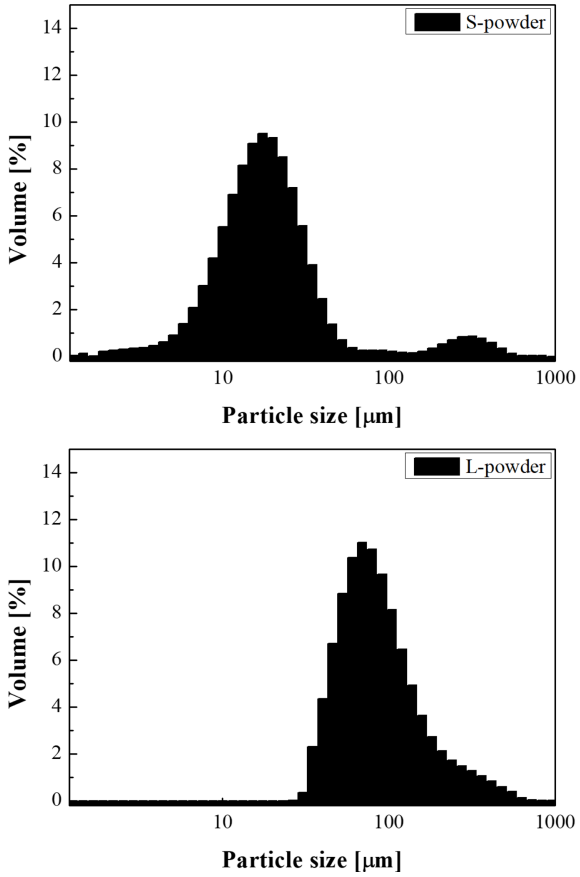

Fig. 2. Laser particle size analysis (LPSA) results according to the powders.

Particle size analysis was conducted to determine the distribution of particles; the results are shown in Fig. 2. S-powder was determined to have the following distribution: D (0.1) = 8.61 μm, D (0.5) = 18.92 μm, and D (0.9) = 43.74 μm. For L-powder, D (0.1) = 42.58, D (0.5) = 74.69 μm, and D (0.9) = 179.67 μm. When the results of the particle size analysis were comprehensively evaluated, each powder was within the target fineness number range and was well distributed into different sizes of powders in different ranges. However, particles with a diameter of approximately 200 μm were also observed. These particles were outside the ranges and had a long rod shape, as shown in Fig. 1; these particles did not form spherical structures during the water-atomization process. These particles were present during the classification by passing through a sieve in a vertical direction.

Figure 3 shows the XRD patterns of the powders with different particle sizes. Regardless of the size difference, in the XRD analysis, both powders exhibited broadened patterns that were typical for amorphous structures. Amorphous particles were fabricated in the powder form before crystallization occurred by rapid cooling through

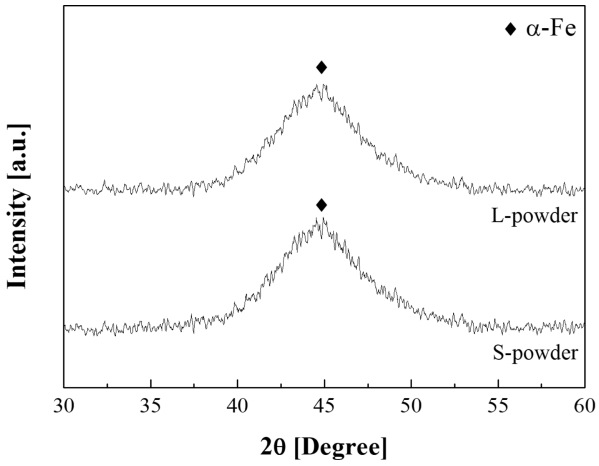

Fig. 3. X-ray diffraction (XRD) patterns of L- and S-powders.

water or gas in liquid state. With an increase in the particle size, a relatively long time was required for the powder to completely cool; the larger the particles, the more time is required for the entire powder to slowly cool and for the crystallization to occur, which simplifies crystallization. However, although the powder used in this study did not have particles larger than 63 μm, all the particles used in this study can be considered to have amorphous structures. The powder produced by water-atomization has been reported to readily form an iron oxide layer on the powder surface; however, because the amount of the iron oxide layer is small, it is not detected by the XRD analysis. This demonstrates that thickness of the iron oxide layer is thin and is a very small percent of the overall fraction. Furthermore, the growth rate of the iron oxide layer on the iron-based amorphous powder is much slower than that of pure iron because the diffusion of iron atoms in an amorphous state is suppressed compared to that in a crystalline state [7]. In addition, although the thicker layers of iron oxide may deteriorate the magnetic properties of the materials, the oxide layer in the powder used in this study was very thin and formed in small quantities; thus, the iron oxide layer will not be detected by XRD.

Figure 4 shows the results of measuring the angle of repose of the powder in the initial single fraction state and of the mixed powder according to the constant mixing ratio. The angle of repose of S-powder in the initial unmixed condition was approximately 42.07 ± 0.97°, and the angle of repose of L-powder was approximately 25.4 ± 1.59°. In addition, it was determined that the angles gradually converged to the angle of repose of a single powder when powders with different particle sizes were mixed. In general, the smaller the size of the particles, the higher the surface energy, and the higher the cohesion

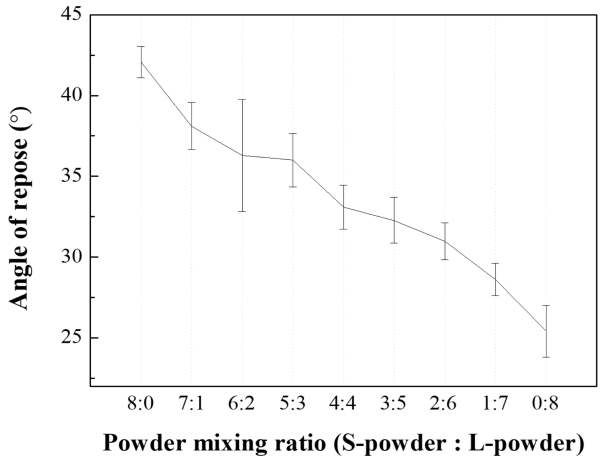

Fig. 4. Change in the angle of repose of the mixed powder according to the set ratio.

[28]. In addition, the surface energy of the powder can be explained by the ratio of the number of atoms placed on the surface and the number of atoms inside the powder. The more atoms are placed on the surface, the lower is the surface energy. Therefore, the higher repose angle of the powder with a relatively small powder size can be measured.

The results of observing the tap density of initial and mixed powders were analyzed and are shown in Table 2. The powder with a smaller particle size is more densely packed in the cylinder, which results in the packing fraction of approximately 72.02 %. However, for large particles, the powders do not easily form pores. The packing fraction of approximately 60.99 % is observed for large pores in the adjacent areas of the powders. The packing fraction of the mixed powder with a 5:3 mass ratio was approximately 73.86 %, which is the highest packing fraction observed. When filling spherical particles of different sizes, which differ slightly depending on the proportion of particle sizes, the optimum weight fraction is approximately 60 % of coarse particles and 40 % of fine particles [22]. However, in this study, 37.5 % of coarse particles and 62.5 % of fine particles were mixed to produce the highest packing fraction. In addition, the powder in this study showed an excellent packing fraction even though the powder did not undergo compression molding or hot forming; the powder was expected to show higher packing density after the forming process. Figure 3 shows the powder with a relatively small particle size. These powders can easily penetrate the pores formed between the cylinder inner walls or between the powders and increase the packing fraction. In addition, with a decrease in the mass ratio of the relatively small particles, the packing fraction slightly increased and gradually decreased above the 5:3 ratio. In general, small particles have a high cohesive force between particles owing to high surface energy, which somewhat lowers the packing fraction. In addition, owing to this property, small particles can easily stick to the inner wall of the cylinder and produce a low packing fraction. Pores with uniform sizes were formed when the powder adhered to the inner wall of the cylinder and to the aggregated powder; these pores had spaces that were difficult to filling by other particles, which lowered the packing fraction. Therefore, fixed pores can be eliminated by mixing powders with different sizes and ratios, which can increase the packing fraction. The maximum packing fraction achieved by monolithic powder and bimodal powder (mixture of small (10-38 μm) and larger (150-250 μm)) has been reported to be 59.39 % and 69.63 % [30]. The highest packing fraction of this study, 73.86 %, can be achieved by optimizing the mixing ratio using the experimental test as well as simulation and analytical modeling.

Table 3 summarizes the powder packing fraction of

Table 2. Change in the tap density test results and packing fraction of mixed powders at a certain ratio.

Mixing ratio S-powder : L-powder	Tap density [g/cm^3]	Packing fraction [%]
8 : 0	4.52	72.02
7 : 1	4.56	72.61
6 : 2	4.62	73.47
5 : 3	4.64	73.86
4 : 4	4.62	73.47
3 : 5	4.53	72.04
2 : 6	4.25	67.68
1 : 7	4.11	65.45
0 : 8	3.83	60.99

Table 3. Polydispersity, skewness, and packing fraction calculated by the Desmond equation and the average diameter of the mixed powder.

Mixing ratio, S-powder : L-powder	Average radius [μm]	Polydispersity, δ	Skewness, S	Packing fraction [%]
8 : 0	10.38	0.63	-0.0176	61.06
7 : 1	15.08	1.22	0.0032	65.04
6 : 2	19.79	1.22	0.0050	65.11
5 : 3	24.49	1.15	0.0032	64.59
4 : 4	29.20	1.06	0.0017	63.97
3 : 5	33.90	0.96	0.0020	63.36
2 : 6	38.61	0.87	0.0018	62.77
1 : 7	43.31	0.79	0.0018	62.20
0 : 8	48.02	0.71	0.0013	61.66

powders with different size distributions, which was theoretically calculated by the Desmond method. The polydispersity and skewness, which considerably affect the packing fraction, are also calculated by the previously described equations. The larger the polydispersity of the particle size distribution, the larger is the variation of the powders. When S-powder is a single powder, the skewness has a negative value. This means that the particle size of the powder is larger than the average particle size. In addition, the packing fraction of the powder at the 8:0 ratio was calculated to be low. Compared to the mixed powder, the fraction of very small particles in a single powder has a greater effect. Therefore, the value of the packing fraction calculated by the skewness value in the Desmond equation was greatly affected and was calculated to be low. Because the powders are mixed, the average radius of the mixed powder increases; thus, polydispersity decreases when the average radius converges to the level similar to that of the relatively large particles. Therefore, the calculated packing fraction is the highest (i.e., 65.11 %) at the 6:2 ratio, and there is a slight difference from the actual experiment value. However, it is confirmed that the packing fraction increases when the powder is mixed, although there is a difference in the overall absolute value.

Table 4 shows the powder packing fraction of powders with different size distributions, which was theoretically calculated by a computer simulation on the basis of DEM-based simulation software. Prior to analyzing the packing fraction for each powder, the conditions were set to be equal to the actual angle of repose and fitted for each factor to implement the angle of repose for the initial powder. The simulation of the angle of repose on S-powder was measured to be approximately 43.02°; it is observed that the angle of repose is within the error range of the measured angle of repose. Similarly, the simulation of the angle of repose for L-powder was determined to be 24.78°, which is within the error range. As described above, fitting was implemented in the software to approximate the properties of the actual powder and to calculate the packing fraction. The packing fraction of powders with small particles was approximately 67.48 %, and the packing fraction of powders with large particles was approximately 64.73 %. The packing fraction of powders with the relatively small particles was higher because when the mold was filled with a single powder, the pores formed by the agglomeration between the powders were relatively small. In addition, different packing fractions were obtained depending on the mixing ratio of the powders. Similar to the tap density results, the highest filling rate of approximately 71.11 % was obtained at the 5:3 ratio; the higher was the fraction of large particles, the lower was the packing fraction. When the fraction of small particles was high, better results were obtained because the higher surface energy of small particles allows the powders to agglomerate well, and when the large particles mix, less aggregated powders and fewer isolated pores are produced. However, a slightly different trend was observed at a 4:4 ratio, which is predicted to have a relatively high cohesive force applied to the S-powder in the simulation, which would have a significant effect on the flow of the L-powder. Powder may reduce the effect of improving the packing fraction due to bi-modal. Powders of the same proportion can receive a relatively large loosening effect [37] due to S-powder particles larger than the space between the particles of the L-powder, and isolated pores formed by the loosening effect of the mixed powder of different proportions are S-powder since filling is possible, it can show a high packing fraction. The discrete element method and the stochastic simulation were more influenced. Similarly, in the experimental result of the loosening effect previously described 4:4 ratio can be observed that the decrease in the packing fraction occurs.

Table 4. Angle of repose of the initial powders and the packing fraction of initial and mixed powders calculated by computational simulation.

Mixing ratio S-powder : L-powder	Angle of repose [°]	Packing fraction [%]
8 : 0	43.02	67.48
7 : 1	-	69.92
6 : 2	-	70.57
5 : 3	-	71.11
4 : 4	-	69.59
3 : 5	-	70.49
2 : 6	-	68.55
1 : 7	-	66.97
0 : 8	24.78	64.73

Figure 5 shows the comparison of the powder packing fraction obtained by the theoretical calculation, experimental measurement, and computer simulation. In the results of experimental packing fraction and simulation, the highest filling rate was observed at the 5:3 ratio, and the highest packing fraction was observed at the 6:2 ratio in the theoretical calculation. These results are similar. The experimental and simulated packing fraction result have maximum values at the mass ratio of 5:3 with similar filling rates over the entire mixing ratio. However, the result calculated by the packing fraction model presented by Desmond shows a lower value than that for other packing fraction (experimental and simulated packing fraction). If the reference packing fraction value is

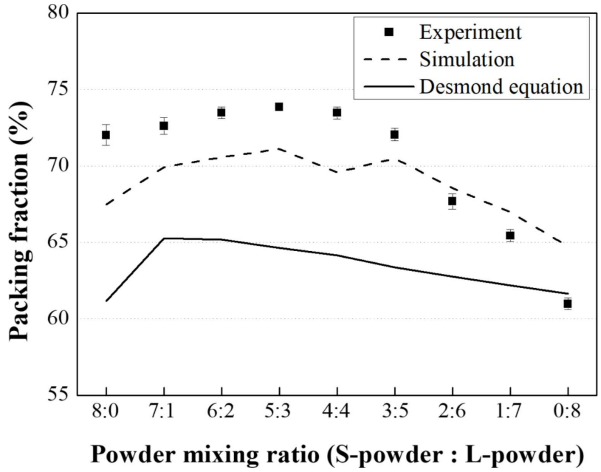

Fig. 5. Experimental packing fraction obtained from tap density and the packing fraction calculated using computational simulation and theoretical equation.

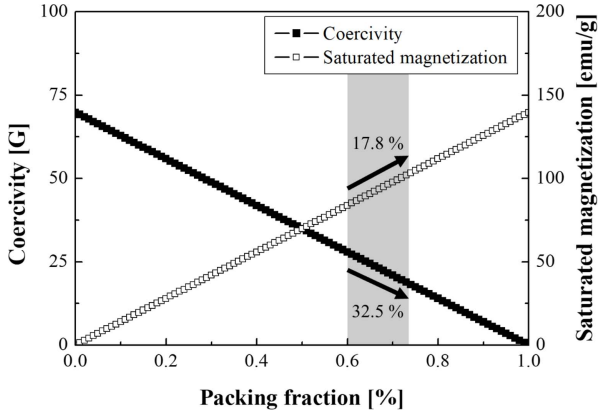

Fig. 6. Changes in coercivity and saturation magnetization calculated by the relationship between packing fraction and magnetic properties.

considered to be an experimental result, the filling rate calculated by the simulation is relatively reasonable, and the packing fraction calculated by the Desmond equation is less valid. For the simulation, various parameters (e.g., particle size distribution of particles) were used to reproduce the experimental angle of repose using the DEM software; the fitting process was performed to accurately implement the powder behavior by reflecting the actual data of the angle of repose. On the basis of the results obtained by the individual DEM method, it is confirmed that the computer simulation produces results that are almost identical to the actual experimental results. In fact, when evaluating the particle size distribution using the simulation, it is determined that small particles fill the gap between large powders, and the pores, which are formed on the sidewall, agree well with the experimental results. However, for the Desmond equation, polydispersity and skewness considerably affect the calculation of the packing fraction. During the powder mixing process, the average radius of the particles converges to the radius of large particles, which reduces polydispersity. It is assumed that the mixed mass ratio that maximizes the filling rate is relatively small compared to the actual test results or computer simulation results. In addition, during the process of deriving the results of the equation, the interaction between the particles and the characteristics of the particles are approximated differently from the actual ones, whereby the equations themselves contain approximate elements.

Figure 6 shows the estimated relationship between the packing fraction and the magnetic properties through the theoretical formula for the magnetic properties of the powder used in this study. The relationship between the packing fraction and the magnetic properties can be expressed through a simple formula, which is shown below:

$$M_r = fM_s \tag{4}$$

$$H_c = \frac{1}{2}(1-f)M_s \tag{5}$$

Where M_r represents the saturated magnetization that depends on the packing fraction, M_s represents the saturated magnetization when the packing fraction is 100 %. In addition, H_c represents the coercivity according to the packing fraction, and f represents the packing fraction of the specimen. When the packing fraction increases from 60.99 % to 73.86 % by mixing the appropriate amounts of smaller particles, the coercivity decreases to 32.5 %, and the saturated magnetization increases to 17.8 %.

4. Conclusion

In this study, we developed a method to increase the packing fraction of soft magnetic amorphous powder. Iron-based amorphous powders with different sizes of particles were mixed at various ratios to determine the optimal mixing ratio, and the powder packing behaviors were also estimated through DEM-based computational and theoretical calculations. In addition, all results were compared to each other to improve reliability. The particle size distribution and the angle of repose measurement were applied to the computational simulation to obtain more valid results. The optimal mixing ratio and computational model presented in this study are expected to improve the performance of products using high-density deformed products during the fabrication of products using soft magnetic amorphous powders.

Acknowledgment

This research was also financially supported from the Civil-Military Technology cooperation program (No.18-CM-MA-15) and by the Ministry of Trade, Industry and Energy (MOTIE) and Korea Institute for Advancement of Technology (KIAT) through the International Cooperative R&D program (P0006837).

References

[1] Market Watch. Soft Magnetic Materials Market Size, Share 2020-Global Industry Trends, Development Insight, Modest Analysis, Statistics, Regional, And Forecast to 2024. Jan. 20, 2020. *https://www.marketwatch.com/press-release/soft-magnetic-materials-market-size-hare-2020-global-industry-trends-development-insight-modest-analysis-statistics-regional-and-forecast-to-2024-2020-01-20*

[2] T. Takahashi, K. Yoshida, Y. Shimizu, A. D. Setyawan, M. Bito, M. Abe, and A. Makino, AIP Advances **7**, 056111 (2017).

[3] A. M. Leary, P. R. Ohodnicki, and M. E. Mchenry, J. Miner. Met. Mater. Soc. **64**, 772 (2012).

[4] S. W. Kim, Y. W. Yoon, S. J. Lee, G. Y. Kim, Y. B. Kim, Y. Y. Chun, and K. S. Lee, J. Magn. Magn. Mater. **316**, 472 (2007).

[5] L. V. Panina and K. Mohri, J. Mag. Soc. Japan. **19**, 265 (1995).

[6] H. Lee, K. J. Lee, Y. K. Kim, T. K. Kim, C. O. Kim, and S. C. Yu, J. Appl. Phys. **87**, 5269 (2000).

[7] Y. J. Lee, J. G. Jeon, S. J. Nam, T. S. Jang, H. J. Kim, M. W. Lee, Y. J. Kim, D. Y. Yang, K. S. Min, and H. J. Choi, Powder Technol. **339**, 440 (2018).

[8] M. A. Nowroozi and H. Shokrollahi, J. Magn. Magn. Mater. **335**, 53 (2013).

[9] A. Makino, T. Kubota, M. Makabe, C. T. Chang, and A. Inoue, Mater. Sci. Eng. B **148**, 166 (2008).

[10] G. Herzer, IEEE. T. Magn. **26**, 1397 (1990).

[11] Y. F. Cui, J. Zhou, and Y. D. Xiao, Mater. Rev. **24**, 27 (2010).

[12] Z. Li, A. Wang, C. Chang, Y. Wang, B. Dong, and S. Zhou, J. Alloys. Comp. **611**, 197 (2014).

[13] Y. Liu, Y. Yi, W. Shao, and Y. Shao, J. Magn. Magn. Mater. **330**, 119 (2013).

[14] G. Herzer, Acta Mater. **61**, 718 (2013).

[15] R. Skomski, Y. Liu, J. E. Shield, G. C. Hadjipanayis, and D. J. Sellmyer, J. Appl. Phys. **107**, 09A739 (2010).

[16] D. Srolovitz, T. Egami, and V. Vitek, Phys. Rev. B **24**, 6936 (1981).

[17] K. W. Park, S. W. Lee, K. H. Kim, and J. C. Lee, J. Kor. Inst. Met. & Mater. **44**, 727 (2006).

[18] K. W. Park, M. Wakeda, Y. Shibutani, and J. C. Lee, J. Kor. Inst. Met. & Mater. **45**, 663 (2007).

[19] E. S. Kim, B. S. Chun, R. Freer, and R. J. Cernik, J. Eur. Ceram. Soc. 30, 1731 (2010).

[20] E. K. H. Li and P. D. Funkenbusch, Metall. Trans. A **24**, 1345 (1993).

[21] C. S. Chen, W. R. Chen, S. C. Chen, and R. D. Chien, Int. Commun. Heat Mass Transfer **35**, 744 (2008).

[22] R. M. German, Particle packing characteristics, Princeton, N. J.: Metal Powder Industries Federation, USA (1989).

[23] S. M. Olhere and J. M. F. Ferreira, Powder Technol. **139**, 69 (2004).

[24] X. Fu, D, Huck, L. Makein, B. Armstrong, U. Willen, and T. Freeman, Particuology **10**, 203 (2012).

[25] S. C. Thakur, H. Ahmadian, J. Sun, and J. Y. Ooi, Particuology **12**, 2 (2014).

[26] J. Schneider and R. Knehans-Schmidt, J. Magn. Magn. Mater. **157/158**, 27 (1996).

[27] J. O'Sullivan, X. L. Rao, and J. M. D. Coey, J. Appl. Phys. **81**, 5124 (1997).

[28] R. Mei, H. Shang, J. F. Klausner, and E. Kallman, KONA Powder Part. J. **15**, 132 (1997).

[29] J. H and Z. Wang, J. Phys: Condens. Matter **7**, 8655 (1995).

[30] J. G. Jeon, S. B. Woo, K. I. No, Y. J. Lee, D. Y. Yang, Y. J. Kim, and H. J. Choi, Korean J. Met. Mater. **54**, 322 (2016).

[31] M. Wang, A. Al-Tabbaa, and W. Wang, Constr. Build. Mater. **229**, 116841 (2019).

[32] M. Wolff, Fabrication and analysis of highly-filled ceramic-polymer composites using the spouted bed technology, Göttingen: Cuvillier, Germany (2015) pp 2-10.

[33] R. Cabiscol, J. H. Finke, and A. Kwade, Powder Technol. **327**, 232 (2018).

[34] X. M. Sun, Y. J. Dong, P. F. Hao, L. Shi, F. Li, and Y. T. Feng, Adv. Powder Technol. **28**, 499 (2017).

[35] K. W. Desmond and E. R. Weeks, Phys. Rev. E **90**, 022204 (2014).

[36] P. A. Cundall and O. D. L. Strack, Géotechnique **29**, 47 (1979).

[37] Y. Knop and A. Peled, Constr. Build. Mater. **102**, 44 (2016).